PHYSICAL REVIEW C VOLUME 40, NUMBER 5 NOVEMBER 1989

Binary decay of ^{56}Ni formed in the ^{32}S$+^{24}$Mg reaction

S. J. Sanders
University of Kansas, Department of Physics and Astronomy, Lawrence, Kansas 66045
and Argonne National Laboratory, Argonne, Illinois 60439

D. G. Kovar, B. B. Back, C. Beck,* D. J. Henderson, R. V. F. Janssens,
T. F. Wang,† and B. D. Wilkins
Argonne National Laboratory, Argonne, Illinois 60439

(Received 19 May 1989)

Fully energy-damped yields from the ^{32}S$+^{24}$Mg reaction have been measured at center-of-mass energies of $E_{\mathrm{c.m.}}=51.6$ and 60.5 MeV with the use of an experimental arrangement where both of the resulting heavy fragments could be detected in coincidence. Energy, velocity, and angular distributions of the reaction fragments have been determined. The cross sections prior to secondary light-particle emission have been deduced for the breakup of the compound system into different mass channels. These data are discussed in terms of two possible reaction mechanisms: fusion followed by fission and deep-inelastic orbiting.

I. INTRODUCTION

The fusion of two heavy ions at energies near the Coulomb barrier generally results in the formation of a compound nucleus which is at a high excitation energy and, on average, has a significant amount of spin. The statistical decay of this compound system into different particle channels then depends in part on the channel and spin-dependent barriers for this decay. For heavier systems the barriers for the symmetric fission channels are often low enough that fission can compete favorably with neutron evaporation for the deexcitation of the compound system. In lighter systems of compound-nucleus mass $A_{\mathrm{CN}}<100$ the low-spin fission barriers are too high for this competition and, in general, most of the compound nucleus deexcitation proceeds through the emission of light particles (n,p,α) and/or γ radiation. The study of how energy and spin are removed from the compound nucleus is important by testing our understanding of the structure of nuclei under extreme conditions of temperature and spin.

Even though suppressed, the emission of fully damped, heavy fragments has been observed in a number of reactions involving lighter systems of total mass $A_{\mathrm{tot}}\leq 60$.[1-12] The breakup of these systems is reminiscent of the fission process as observed in heavier systems, but shows some characteristic differences as well. In lighter systems the breakup seems to occur only for the higher-reaction partial waves and, at least for energies which are not too high, an asymmetric mass splitting seems to be favored.[11] These yields have been discussed both in terms of fusion-fission[4,7,9,15,17,18] and deep inelastic orbiting mechanisms.[1-3,5,8,10,13,14,16] Since the compound-nucleus scission shapes for lighter systems are expected to look very much like two touching spheres,[19,20] the experimental signatures which can be used to distinguish between these two pictures are not obvious and it is possible that both mechanisms are present.[14,15]

In this paper we present results for the binary breakup of the ^{56}Ni system as populated through the ^{32}S$+^{24}$Mg reaction. Data were obtained at two beam energies, $E_{\mathrm{beam}}=121.1$ and 141.8 MeV, using the Argonne National Laboratory ATLAS facility. By detecting both fragments in coincidence it was possible to deduce the primary mass distribution for the breakup process before secondary light-particle emission from the fragments. The energy and mass distributions were determined as functions of angle to show the fully damped nature of the breakup process. These data were then compared to the results of model calculations of the fusion-fission process as well as the deep-inelastic scattering process. We conclude that a statistical fission model, which incorporates newer estimates of the saddle-point energies as a function of mass asymmetry and spin, describes the experimental results satisfactorily. The equilibrium model of orbiting, developed for systems of total mass $A\leq 42$ by Shivakumar *et al.*,[8,10] is found to also give reasonable agreement with the data if it is extended to allow for the deformation of the orbiting nuclei.

The primary, preevaporation mass distribution which is deduced from the coincidence data shows that mass asymmetric channels are favored. This is expected for fission of a light nucleus where the fission potential-energy surface becomes unstable against asymmetric deformations.[20,21] Although it was not possible to obtain coincidence data for the ^{8}Be$+^{48}$Cr channel, and only limits could be set on the total ^{8}Be cross section, an estimate of the ground-state cross section in this channel could be obtained from our singles data.

The paper is organized as follows: The experimental arrangement is discussed in Sec. II. The characterization of the singles data is presented in Sec. III. We will present the results of the coincidence data and the simulations which allow us to deduce the primary mass distributions for the binary-decay process in Sec. IV. In Sec. V the results for the ^{8}Be channel will be presented. The results of a statistical-fission-decay calculation incorporating recent estimates of the mass-asymmetry-dependent fission barriers for ^{56}Ni will be discussed in Sec. VI. Possible alternative models will be presented in Sec. VII. We conclude with an assessment of the importance of these yields in understanding the fusion of light nuclear systems. Some of the results presented here have been previously reported in shorter papers[11,22] (although the cross sections quoted here supersede those in the earlier papers).

II. EXPERIMENTAL ARRANGEMENT

The basic experimental arrangement, shown schematically in Fig. 1, consisted of five Si (surface barrier) detectors located on one side of the beam axis and two Breskin-type[23] transmission, position-sensitive multiwire proportional counters mounted on the opposite side. Beams of 121.1 and 141.8 MeV ^{32}S from the Argonne National Laboratory ATLAS facility were used to bombard a 160 μg/cm^2 self-supporting ^{24}Mg target. The five Si detectors measured the energies and flight times of the reaction products, from which the masses of these products could be derived. The subtended solid angles, laboratory angles, and distances of these five detectors were 0.26 msr (8°, 86.7 cm), 0.36 msr (16.3°, 73.3 cm), 0.74 msr (28.1°, 40.0 cm), 1.54 msr (38.2°, 35 cm), and 2.91 msr (48.2°, 35 cm), respectively. The two gas counters established the velocities of the recoiling fragments by measurements of position and time of flight. These counters, of active area 8 cm$\times$9 cm and located 32.3 and 14.2 cm from the target, respectively, covered in-plane angular openings of 16° and 31°. In two angular settings the recoil range of $6° \leq \theta_{\text{recoil}} \leq 91°$ was covered completely.

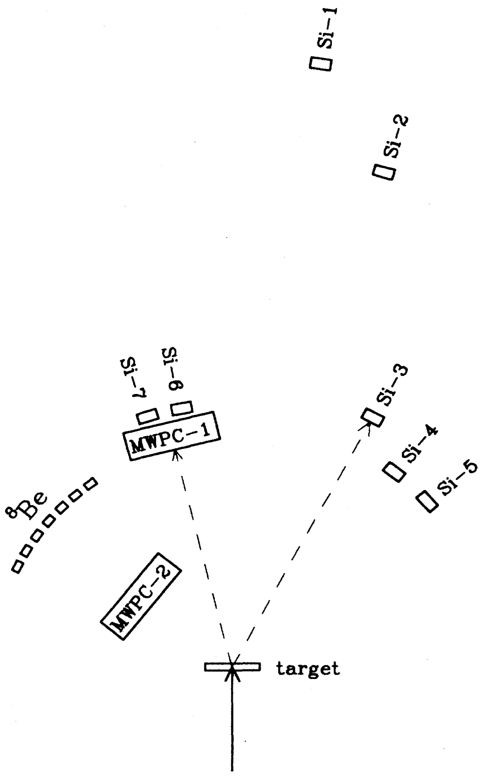

FIG. 1. Schematic drawing of the experimental setup. The primary heavy-fragment detectors are denoted Si-1 through Si-5. The two multiwire gas proportional counters, MWPC-1 and MWPC-2, are backed by additional Si detectors. Those detectors behind MWPC-2 comprise the ^{8}Be detection array. See text for details.

Additional Si detectors were located behind the proportional counters. They were used in the calibration of the latter. Two detectors were mounted behind the forward gas counter and an array of seven rectangular (0.9 cm$\times$4.8 cm) Si detectors, located 21.3 cm from the target, backed the larger-angle gas counter. The detectors in the array were mounted with a 2° gap between their active areas and had an angular acceptance of about 2.5° each. In addition to being used in the calibration of the large-angle gas counter, these seven detectors also served to obtain an estimate of the ^{8}Be ground-state cross section by measuring both of the alpha particles from the ^{8}Be decay in coincidence (the ground state of ^{8}Be is unbound by 92 keV for alpha-particle breakup).

The energy calibrations of the Si detectors were obtained by measuring the elastic scattering of a 59.5-MeV ^{16}O beam off of ^{24}Mg, ^{40}Ca, and ^{197}Au targets. Additional calibration points were obtained by the 5.5-MeV alpha-particle line from an ^{241}Am source and, for those detectors at angles less than or close to the grazing angles at the two different beam energies, for elastic scattering of the ^{32}S beam off of the ^{24}Mg and ^{197}Au targets. The linearity of the electronics was checked using a precision pulser. All energies quoted in this paper (except for the incident, laboratory beam energies which are given at the entrance to the target) have been corrected, where appropriate, for the target thickness, energy loss in the Au layer on the Si detectors, pulse-height defect in the Si detectors (using the Kaufman prescription[24]), and losses in traversing the foils of the gas counters (only for the shadowed detectors).

The cross-section data were normalized by fitting the observed ^{32}S+^{24}Mg elastic scattering angular distributions with cross-section predictions for these distributions using the distorted-wave Born approximation (DWBA) code PTOLEMY.[25] The uncertainty in this normalization procedure, which would lead to a systematic shift in all of the quoted cross sections, is believed to be less than 10%.

Mass identification was achieved by the time-of-flight technique using the pulsed nature of the ATLAS beam. The time width of the beam pulses was approximately 350 ps, with a separation between pulses of 81.6 ns. After a first-order linearization of the data to obtain mass lines using the expression $M \propto E \times T^2$, where E is the particle energy and T is the time of flight, the final mass calibrations were achieved by an interactive linearization of the $(E \times T^2)$ vs E spectra. In Fig. 2 the resulting mass calibration for the 8° detector at $E_{\text{beam}} = 141.8$ MeV is shown

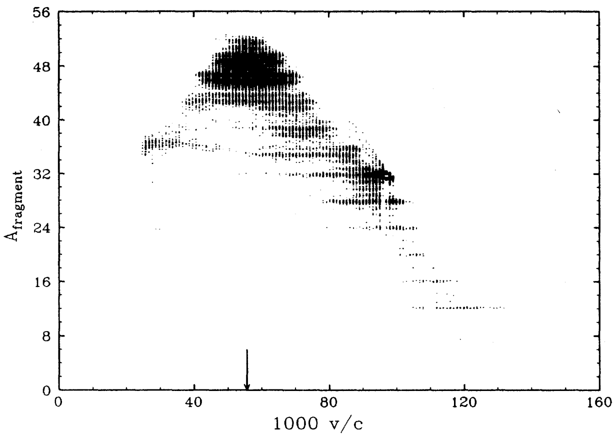

FIG. 2. Mass versus velocity spectrum for the $^{32}S+^{24}Mg$ reaction at $E_{\text{c.m.}}=60.5$ MeV and $\theta_{\text{lab}}=8°$. The center-of-mass velocity, $v_{\text{c.m.}}$, is indicated by the arrow. (The mass calibration for $A_{\text{fragment}}<40$ and $v<v_{\text{c.m.}}$ is not reliable because of uncertainties in the energy corrections for these low-velocity fragments. Elastic pileup counts have been suppressed, resulting in the gap seen for the mass lines with $24 \leq A \leq 32$.)

in terms of a two-dimensional mass versus velocity plot. For this forward-angle detector, unit mass resolution is achieved up through the evaporation-residue channels. (These are seen to be centered at the center-of-mass velocity.) In Fig. 3 the inclusive mass spectrum is shown for the 28° detector at 141.8 MeV. The mass resolution is somewhat worse for this large-angle detector, but individual masses can still be identified up through the beam mass of 32.

The velocity spectra shown in this paper for the Si detectors are based on the fragments energies and masses. For the gas counters, velocities are based on the measured flight times and known distances to these counters, with the time calibrations achieved using the backing Si detectors to identify elastically scattered beam particles. The time calibrations for the gas counters were found to have only a weak position dependence, and no correction for this dependence was made. The detectors used to measure the ^{8}Be-breakup alpha particles were too thin to stop these light particles, but clear mass identification was still possible from the correlated energy and time information. The quoted alpha-particle energies in these detectors are therefore based on the particle flight times.

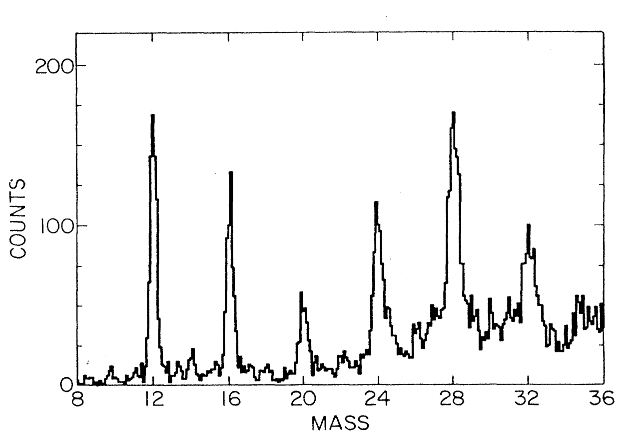

FIG. 3. Mass spectrum for the $^{32}S+^{24}Mg$ reaction at $E_{\text{c.m.}}=60.5$ MeV and $\theta_{\text{lab}}=28.1°$.

III. INCLUSIVE MEASUREMENTS

In this section we will restrict our discussion to the inclusive data obtained using the five forward-angle Si detectors. In general we can characterize the observed heavy-ion fragments as arising from one of three distinct classes of reactions: (1) the evaporation-residue yields following light-particle emission from the compound nucleus, (2) the elastic and quasielastic yields in mass channels near to the projectile mass, and (3) the binary, fully damped reaction yields.

The different components of the total reaction cross section are evident in the mass versus velocity distribution shown in Fig. 2. The distribution shows a transition from light-particle evaporation from the compound system (where the velocities are centered at the velocity of the center of mass) to binary breakup processes where, for the heavier particles, there are two kinematic solutions (resulting from the fragment velocity in the center-of-mass system being less than the velocity of the center of mass). In this figure the low-velocity part of the distribution is truncated around mass 32 by the detector energy threshold. For masses less than 44, the yield centered around the center-of-mass velocity largely disappears and all of the cross section corresponds to binary processes. Between mass 12 and 24 the yields are fully energy damped, i.e., the total kinetic energy is comparable to the potential energy of the two nuclei in a near-touching configuration. The reaction products corresponding to more peripheral collisions, the elastic and quasielastic processes, are localized around the projectile mass of 32. The saturation of the density scale in Fig. 2 tends to understate these yields; however, the importance of the α-pickup process is clearly evidenced by the high-velocity peak in the mass 36 line.

An enhanced cross section in every fourth mass channel up through the projectile mass of 32 is clearly seen in both Figs. 2 and 3. This enhancement can be attributed to the greater binding energy of the "alpha-particle-like" nuclei ^{12}C, ^{16}O, ^{20}Ne, etc., and indicates that shell effects play an important role in the breakup of the compound system.

Angular distributions of $d\sigma/d\theta$ are shown for the stronger mass channels up through the symmetric-breakup channel of mass 28 in Fig. 4. Except for the symmetric mass 28 channel, these cross sections are found to be largely angle independent (with $d\sigma/d\Omega \propto 1/\sin\theta_{\text{c.m.}}$) as expected for the decay of a spinning compound nucleus in the plane perpendicular to the spin vector. Forward-angle enhancements are seen for the mass 28 channel at both energies, however. This suggests that in this near-projectile mass channel there is a more peripheral component to the reaction cross section.

Evidence that the mass 28 channel may contain contributions from more peripheral reaction processes can also be deduced from the average total kinetic energies ($\langle E_{K,\mathrm{tot}} \rangle$). This is shown in Fig. 5, where the $\langle E_{K,\mathrm{tot}} \rangle$ values are indicated for the dominant mass channels as a function of scattering angle. Two-body kinematics were assumed in deriving these energies. The average values of $E_{K,\mathrm{tot}}$ for the mass 12, 16, 20, and 24 channels are found to be angle independent as expected for a fully damped process. However, for the mass 28 channel the $\langle E_{K,\mathrm{tot}} \rangle$ values are found to increase at forward angles suggesting less dissipation of the entrance-channel energy into internal excitation of the fragments. For angles greater than 60° ($\theta_{\mathrm{lab}} > 28°$) all of the observed cross section corresponds to the fully damped processes and, as a consequence, the mass distribution shown in Fig. 3 for a single angle reflects the relative mass abundances of the angle-integrated cross sections for these processes.

What cannot be demonstrated from the singles data is the degree to which the observed mass distribution is affected by secondary light-particle emission from the reaction fragments, or the extent to which nonbinary processes affect the measured distribution. To explore these issues we used the gas counters mounted on the opposite side of the beam axis to detect the recoiling reaction fragments. These coincidence measurements are discussed in the next section.

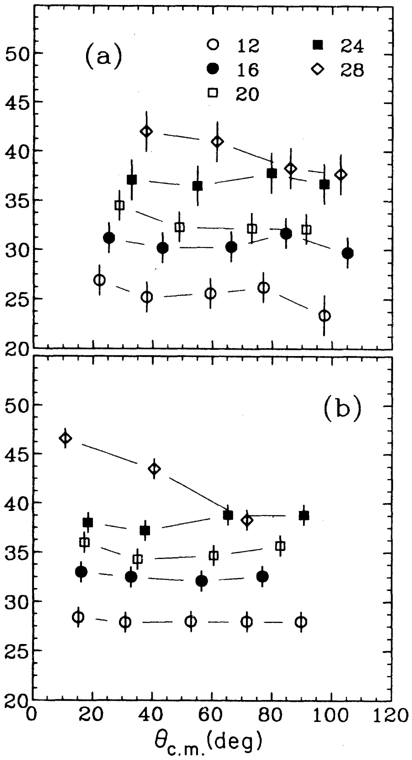

FIG. 5. Angular dependence of the average total kinetic energies $\langle E_{K,\mathrm{tot}} \rangle$ for the $^{32}\mathrm{S}+^{24}\mathrm{Mg}$ reaction at $E_{\mathrm{c.m.}} = 51.6$ (a) and 60.5 MeV (b).

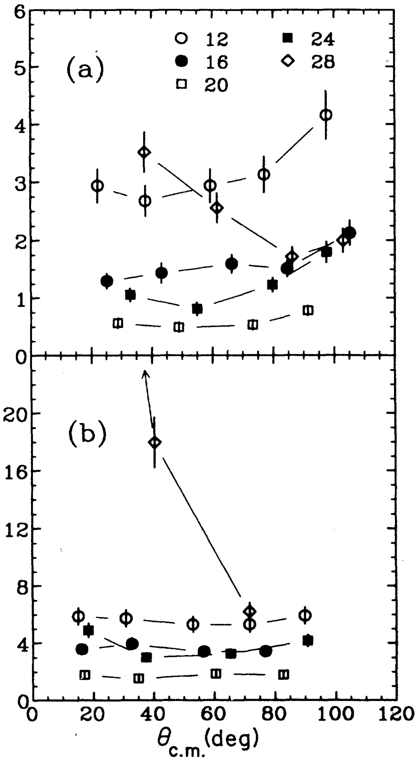

FIG. 4. Angular dependence of cross section $d\sigma/d\theta$ for the $^{32}\mathrm{S}+^{24}\mathrm{Mg}$ reaction at $E_{\mathrm{c.m.}} = 51.6$ (a) and 60.5 MeV (b).

IV. COINCIDENCE MEASUREMENTS

In studying the fully damped binary yields, the detection of both heavy fragments originating from the breakup of the compound system is essential if one wants to establish the two-body nature of the reaction. It also helps in the deduction of the primary, preevaporation mass distribution for the process. It is possible that one or both of the reaction products will be left with sufficient excitation energy for secondary light-particle emission. The coincident detection of both of the resulting heavy fragments can be used to estimate the extent to which this secondary evaporation modifies the observed mass distribution from the original, preevaporation distribution. In the present experiment, the secondary light-particle emission from the fragment identified in the Si detectors is found to depend strongly on the mass of the original fragment, with little or no evaporation found for mass 12, but substantial evaporation seen for some of the heavier identified fragments corresponding to the more symmetric-decay channels. The energies of the present measurements are sufficiently low that, in general, the emission of only one light particle is possible for fragments up through mass 32. This low multiplicity simplifies the modeling of the decay process by Monte

Carlo techniques.

With our experimental setup we were able to determine the velocity vectors of both of the final heavy fragments from the breakup of the compound system. For one of the fragments (that detected in the Si detectors), we could also determine the mass. The overall efficiency for the coincident detection of both fragments depends on the relative angles of the detectors. In our analysis of the coincidence data we concentrate on the results of the $\theta_{\text{lab}}=28.1°$ Si detector since essentially only binary, fully damped reaction yields are emitted at this angle and the corresponding recoil angles are completely covered by the gas counters in one or the other of their two settings. The coincidence efficiency for the 28.1° detector was found to be better than 80% for masses $12 \leq A_{\text{fragment}} \leq 28$, as determined by comparing the mass spectra for this detector with and without the coincidence requirement.

The center-of-mass folding angles are shown in Fig. 6 for the stronger mass channels seen in the $\theta_{\text{lab}}=28.1°$ detector at $E_{\text{c.m.}}=60.5$ MeV. These distributions were obtained by an event-by-event conversion of the laboratory velocities of the two detected fragments to the center-of-mass system based on the known velocity of the center of mass. For a two-body reaction, without secondary light-particle evaporation, the distributions should peak sharply at 180°. Secondary light-particle evaporation from either of the reaction fragments will lead to a broader distribution of folding angles (but still centered at 180°). Since the conversion to the center-of-mass system assumes a specific reaction, the centroids of the folding-angle distributions for target contaminants will be shifted away from 180°. This is clearly seen in the spectrum for mass 32 where several peaks corresponding to heavy-target contaminants are found at larger folding angles. Yields arising from lighter contaminants (^{12}C, ^{16}O) will appear at smaller angles and some evidence for this is seen in the low-angle tails of the distributions. Of principal concern for these measurements would be the presence of significant amounts of carbon or oxygen since either of these contaminants could possibly lead to enhanced yields at large angles in the more mass-asymmetric channels (i.e., mass 12 or 16) through a molecular-resonance process.[26] These contributions are small, however, and do not affect our analysis significantly. No specific correction for these yields has been attempted.

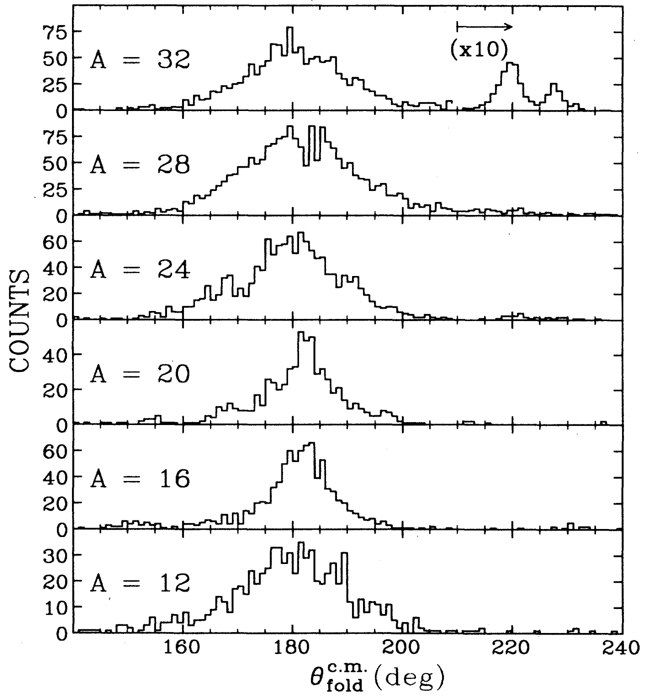

FIG. 6. Center-of-mass folding-angle distributions for the ^{32}S+^{24}Mg reaction at $E_{\text{c.m.}}=60.5$ MeV and $\theta_{\text{lab}}=28.1°$. The distributions are shown for various fragment masses.

Since the folding-angle calculation assumes full momentum transfer, processes involving incomplete momentum transfer to the compound nucleus will also shift the distributions away from 180°. Contributions from these processes are also seen to be very small, if present at all. This result is consistent with the systematics for incomplete fusion.[27]

Momentum conservation can be used to deduce the primary (preevaporation) fragment masses. For decay fragments labeled 3 and 4 of mass M_3 and M_4 and velocities $v_3^{\text{c.m.}}$ and $v_4^{\text{c.m.}}$ in the center-of-mass system, momentum conservation gives $M_{3(4)}=M_{\text{tot}}\times v_{4(3)}^{\text{c.m.}}/(v_3^{\text{c.m.}}+v_4^{\text{c.m.}})$, where M_{tot} is the compound system mass 56. Secondary light-particle emission will result in a distribution of masses around the actual, discrete value of the primary fragment mass, but will not shift the average value from that of the primary mass. The mass distributions obtained for the primary, preevaporation masses of fragments detected in the 28° detector at $E_{\text{c.m.}}=60.5$ MeV are shown in Fig. 7 (bold histograms) for the

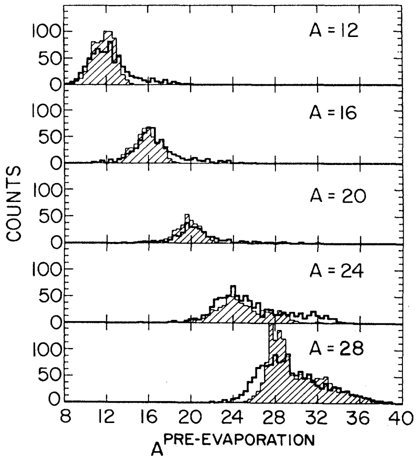

FIG. 7. Preevaporation mass distributions derived from the measured fragment velocities for different regions of the observed mass spectrum at $\theta_{\text{lab}}=28.1°$ (bold histograms) and the corresponding mass spectra obtained from the LILITA calculations as described in the text (shaded histograms).

stronger observed (post-evaporation) mass lines up through the symmetric mass 28 channel. From this figure it is evident that the observed mass distribution is most strongly affected by secondary emission in the more symmetric mass channels of $A=24$ and 28, while little evidence of secondary evaporation is found for the lighter mass channels. In these two channels, however, a significant amount of the observed yields is found to result from heavier fragments which undergo light-particle emission. A lesser, but still significant, amount of secondary evaporation is found for the data obtained at the lower beam energy with $E_{\mathrm{c.m.}}=51.6$ MeV.

To deduce the actual, preevaporation mass distribution at the two beam energies, the Monte Carlo code LILITA (Ref. 28) was used to simulate the evaporation process. A detailed description of these calculations can be found in Ref. 11. Briefly, a specific primary mass distribution is assumed as input to the calculation. The LILITA code then follows the statistical light-particle decay of the fragments and, on an event-by-event basis, gives the final masses and velocities of the post-evaporation heavy ions. These results can then be compared with the experimental data, which may lead to a new iteration on the assumed primary mass distribution, if necessary.

Examples of the data fitted by LILITA are shown in Figs. 7–9. The shaded histograms in Fig. 7 were obtained using LILITA to calculate the preevaporation masses based on the final (post-evaporation) velocities. The assumed mass distribution leads to a good reproduction of the experimental results. In Fig. 8 we show the observed velocity spectra for some of the stronger mass channels at 8° and 28.1° at the higher beam energy as well as the LILITA simulations of these spectra. At the larger-angle good agreement is achieved for all masses. Significant differences are observed between the measured and calculated distributions at 8°, however. These differences are attributed to the presence of more peripheral processes in the near projectile/target masses at the more forward angle, as indicated earlier in the discussion of the singles data.

Finally, the experimental mass distributions at the two beam energies for that component of the reaction yield consistent with a $1/\sin\theta_{\mathrm{c.m.}}$ angular dependence are shown in Fig. 9 by the open histograms. (The data have been binned every second mass at the lower energy because the reduced cross sections at this energy made it difficult to resolve the weaker channels.) The preevaporation mass distributions needed by LILITA to reproduce these results are also shown in the figure. Most of the cross-section enhancement observed for the more symmetric mass channels at the higher beam energy can be attributed to secondary light-particle evaporation from even heavier masses. At the lower beam energy the secondary evaporation process still modifies the mass spectrum, but to a lesser extent. A mass-asymmetric breakup process is evident at both energies, with increased importance of the asymmetric component at the lower energy.

The general trend of these results raises the question of the magnitude of the breakup cross section in the mass $A=8$ channel. Binding-energy considerations suggest that the dominant mass 8 nucleus should be ^{8}Be. These events, however, would only be separable from alpha-particle evaporation in the forward-angle detectors if both α particles from the ^{8}Be decay would reach a single detector, rendering the efficiency for identification very low. In the next section, however, it is shown that some information about the ^{8}Be channel can be obtained from the closely spaced Si detectors behind the back gas counter.

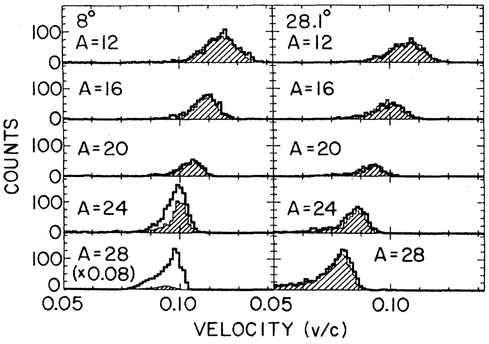

FIG. 8. Measured velocity spectra (bold histograms) and the corresponding LILITA simulations (shaded histograms) at $E_{\mathrm{c.m.}}=60.5$ MeV and $\theta_{\mathrm{lab}}=8°$ and 28.1°.

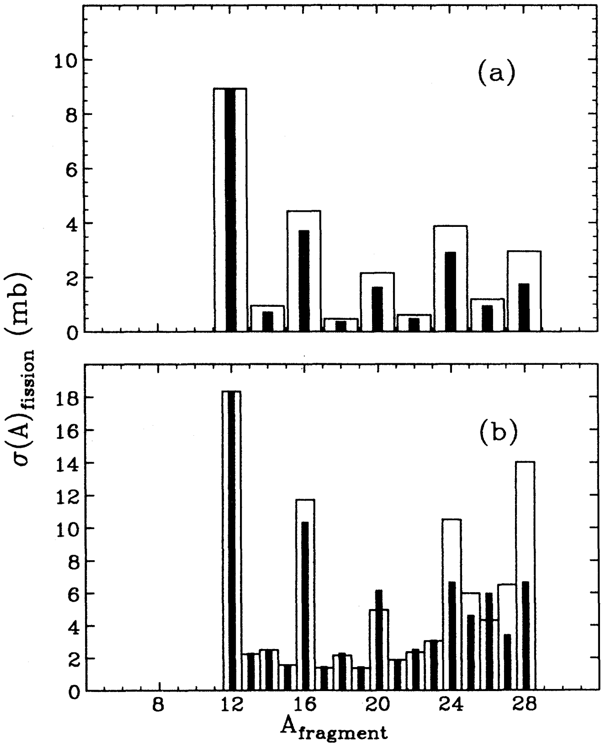

FIG. 9. Observed mass distributions (open histograms) and the corresponding deduced pre-evaporation mass distributions (solid histograms) for the fissionlike component of the ^{32}S $+^{24}$Mg reaction at $E_{\mathrm{c.m.}}=51.6$ (a) and 60.4 MeV (b).

V. ^{8}Be EMISSION

One method for ^{8}Be identification is to detect in coincidence the two α particles from its decay. Cross sections are then deduced from simulations of the detector response based on assumed properties of the ^{8}Be production and decay. This was done at the two different beam energies using the seven, closely spaced detectors located behind the rear gas counter. The failure of an electronics module during the experiment resulted in the ^{8}Be data being obtained at different angles of the back gas counter (and Si detector array) for the two beam energies. At $E_{\mathrm{c.m.}}=51.6$ MeV the seven detectors covered the angular range $36.5° < \theta_{\mathrm{lab}} < 63.8°$ and at $E_{\mathrm{c.m.}}=60.5$ MeV, only six of the detectors were used covering the angular range $66.5° < \theta_{\mathrm{lab}} < 90.5°$ (at the higher energy the most backward detector was shielded by the target frame).

The relative momentum p_{rel} of coincident alpha particles hitting any two of the seven strip detectors is shown in Fig. 10 for the two beam energies. In each of these momentum spectra there is an enhanced yield centered near $p_{\mathrm{rel}}=37$ MeV/c, corresponding to the detection of two alpha particles from the breakup of the ^{8}Be ground state. The width of this peak results from the uncertainty in the angle measurement with the present experimental setup. The counts at higher values of p_{rel} can arise from two sources: the production of ^{8}Be in an excited state and the sequential emission of alpha particles from the compound nucleus. It is not possible with the present experimental setup to distinguish between these two processes.

The low p_{rel} peaks in the spectra at the two energies were simulated by a Monte Carlo calculation of the ground-state ^{8}Be decay process, where it was assumed that the ^{8}Be is emitted with an angular distribution given by $d\sigma/d\Omega \propto 1/\sin\theta_{\mathrm{c.m.}}$. The subsequent α-particle breakup is assumed to be isotropic in the ^{8}Be center-of-mass system. To calculate the reaction kinematics, Gaussian distributions were assumed for the total kinetic energy $E_{K,\mathrm{tot}}$ with the mean (standard deviation) for the distributions taken as 23 MeV (5 MeV) and 25 MeV (5 MeV) at $E_{\mathrm{c.m.}}=51.6$ and 60.5 MeV, respectively. The results are relatively insensitive to these values: changing the values of $\langle E_{K,\mathrm{tot}}\rangle$ by ± 2 MeV results in a noticeable shift in the centroid of the distributions, but only slightly

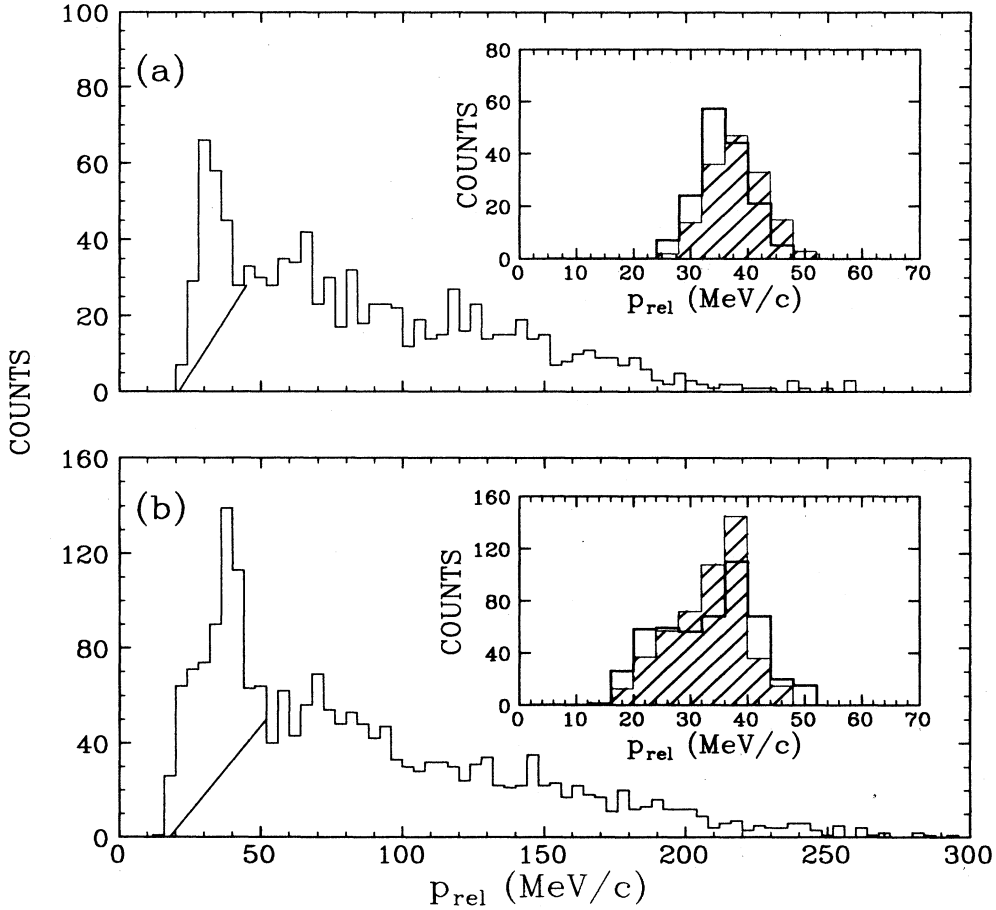

FIG. 10. Relative momentum of two alpha particles hitting the Si detector array behind the rear gas counter MWPC-2 at $E_{\mathrm{c.m.}}=51.6$ (a) and 60.5 MeV (b). The subpanels show the results of Monte Carlo simulations of the alpha-particle breakup of the ^{8}Be ground state (crosshatched histograms) compared to the data (bold histograms), as discussed in the text.

changes the value of the deduced ^{8}Be cross sections. The simulated spectra are compared to the $p_{\rm rel}$ peaks, after the linear backgrounds, as shown, have been subtracted, in the subpanels of Fig. 10.

The ground-state ^{8}Be cross sections deduced from these simulations of the decay process are 2 ± 1 and 5 ± 2 mb at $E_{\rm c.m.}=51.6$ and 60.5 MeV, respectively. The much larger total cross sections for the ^{8}Be channel of 70 and 100 mb at the two energies, respectively, suggested in Ref. 22, correspond to treating all of the higher $p_{\rm rel}$ values as resulting from the excited-state decay of ^{8}Be. This sets an absolute upper limit on the ^{8}Be cross section. A thermal population[29] of ground- and first-excited states in ^{8}Be from ^{56}Ni decay would suggest total cross sections of about twice the ground-state values. Because of the large uncertainty in the total ^{8}Be cross section, we do not show these values for comparison with the subsequent model calculations. Our experimental results suggest, however, substantial cross sections in the ^{8}Be channel, at a level similar to that found for the ^{12}C and ^{16}O channels, but probably not significantly higher than that found in these channels.

VI. FUSION-FISSION MODEL CALCULATIONS

In describing the compound-nucleus fission process we utilize the transition-state model,[20,30] which has a long history of success in describing fission decay in heavier systems. In this model the probability of decay by fission is proportional to the available phase space above the saddle point, i.e., the point where the angular-momentum-dependent potential energy associated with the shape of the nucleus reaches a maximum. In heavier systems the nucleus is stable against asymmetric mass deformations and the symmetric-saddle-point energy is used in fission calculations. In contrast, lighter nuclei become unstable against asymmetric deformations and the mass-asymmetry-dependent saddle-point energies are needed to calculate fission competition. In a simplified treatment, the transmission coefficients for fission decay are typically assumed to be zero at energies less than the saddle-point energy, and at unity above this energy. The competing process of light-particle emission is treated in terms of the standard Hauser-Feshbach formalism: the decay probability is taken to be proportional to the level densities in the accessible evaporation residues weighted by the appropriate optical-model transmission coefficients. The apparent dichotomy between fission and light-particle evaporation, which is inherent in this picture, is a consequence of the fact that the fission barrier is more compact than the scission configuration in the heavy systems for which this model was developed. It has been shown,[21] however, that this description naturally extends to the lighter systems, where the point of minimum excitation energy and the scission point are closer together, as is the case in light-particle evaporation processes.

We have applied the transition-state theory to the fission decay of the ^{56}Ni compound nucleus. The calculations were done using spin- and mass-asymmetry-dependent fission barriers incorporating finite-nuclear-range and diffuse-surface effects. In general, these barriers are not available in the literature, although a detailed discussion of how they might be calculated has been outlined in a series of papers by Davies, Krappe, Nix, and Sierk.[19,31]

Here we have closely followed the work of Sierk[19] in calculating saddle-point energies for ^{56}Ni. The calculations were performed assuming a shape parametrization in terms of three, connected, quadratic surfaces of revolution. A minimization procedure was employed to find the stationary points of maximum energy of the potential-energy surface; the resulting saddle-point energies are shown in Fig. 11. For the limiting case of fission to a massless particle, the saddle-point energy is taken as the equilibrium energy for ^{56}Ni at the appropriate spin value, as tabulated by Sierk.[19] Some interpolation was necessary between this extreme and the minimum mass asymmetry for which the asymmetric-saddle-point calculations converged, usually corresponding to a fragment mass of $A_{\rm fragment}\sim12$. (At larger mass asymmetries our calculations either did not converge, or found stationary points which did not correspond to a true, asymmetric saddle point with only two normal modes of unstable equilibrium.) The fission barrier at a given mass asymmetry and spin then corresponds to the difference in energy between the equilibrium value and the corresponding saddle-point energy. In Fig. 11 we have also noted the symmetric-saddle-point calculations of Sierk[19] for spins 0, 28, and 36. Good agreement is found comparing the two calculations. The moments of inertia found in our calculations for the symmetric shapes (typical shapes are shown in the figure) were also in very good agreement with the earlier results of Sierk.[19]

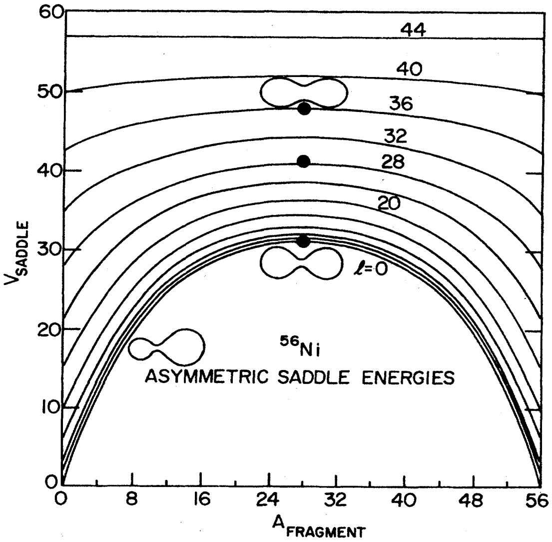

FIG. 11. Saddle-point energies for the ^{56}Ni compound nucleus as a function of spin and mass asymmetry. The mass-asymmetry coordinate is given by the final fragment mass assuming fission occurs. Also indicated are the energies previously obtained by Sierk (Ref. 19) for the symmetric barriers at spins $J=0$, 28, and 36.

One check on the general validity of the saddle-point calculations is to compare the predicted value of the total kinetic energy of the system after fission with the corresponding experimental values. In light systems the scission and saddle points are believed to be very close in energy[32] and therefore the saddle-point potential energy should be comparable to the total asymptotic kinetic energy after breakup. By approximating the symmetric-saddle-point configuration at spin $J=36\hbar$ with two spheroids, we can calculate the relative potential energy of these spheroids. (As shown below, symmetric fission at $E_{\mathrm{c.m.}}=60.5$ MeV is expected to occur for partial waves near $l=36\hbar$.) The calculated value of $E_{K,\mathrm{tot}}=38.4$ MeV is in good agreement with the experimental value of 38.0 ± 1.5 MeV.

The saddle-point energies shown in Fig. 11 were incorporated into the statistical evaporation code CASCADE (Ref. 33) by assuming the probability of fissioning into a given mass partition to be proportional to the level density above the generalized saddle point (the "ridge" line in Moretto's notation[21]). It is evident from the mass distributions shown in Fig. 9, where every fourth mass has an enhanced cross section, that shell effects are significant in the breakup process. To include these effects in the calculations, the mass-asymmetric saddle-point energies were adjusted by a term given by the sum of the Wigner energy terms[34] for the two fragments. This correction, which does not affect the barrier energies used for the decay to two even-even nuclei, results in an energy penalty against the decay to channels containing even-odd or odd-odd nuclei.

The CASCADE mass predictions for the fission channels at the two beam energies are compared to the data in Fig. 12. In these calculations the saddle-point energies were used for the breakup of the compound nucleus to fragments as light as mass 6, and only first-chance fission was allowed. The competing process of light-particle emission (p,n,α) was handled normally using the evaporation-residue level densities. Saddle-point level densities were calculated using the Fermi gas expression given in Ref. 35, with the available energy taken as the difference between the compound-nucleus excitation energy and the mass-asymmetry and angular-momentum-dependent saddle-point energy. For these calculations the rigid-body moment of inertia was obtained by assuming a two-spheroid approximation to the saddle-point shape. The fusion partial cross sections were taken as

$$\sigma_l^{\mathrm{fus}}\sim(2l+1)/\{1+\exp[(l-l_0)/\Delta]\}\ ,$$

where l_0 is the angular-momentum cutoff parameter for fusion and Δ is the corresponding width parameter. The level density, angular momentum, and width parameters were adjusted to give the best overall fit to the fission mass distribution while still being consistent with the experimentally determined systematics for evaporation-residue cross sections[36] at these energies. Between the two energies, only the l_0 parameter was varied (resulting in calculated *total* fusion cross sections of 1047 and 1123 mb at $E_{\mathrm{c.m.}}=51.6$ and 60.5 MeV, respectively). A width of $\Delta=1\hbar$ was found to give reasonable results at both energies. The level-density parameters for the fission and evaporation-residue channels were taken as $A/9.3$ and $A/8.0$, respectively.

As seen from the figure, good agreement is found between the calculated and measured mass distributions for $A_{\mathrm{fragment}}\geq12$. This is more clearly displayed in Fig. 13 where the experimental cross sections for the stronger mass channels are shown with the CASCADE predictions for these channels. Also shown are the calculated cross sections for the first-chance evaporation of nucleons (sum of neutron and proton) and α particles. The discontinuous behavior of the calculated curve between masses 4 and 8 can be attributed to a change from an evaporation-residue, post-scission phase space to the fission, saddle-point phase space.

The ratio of the level-density parameters used to achieve these fits, $a_f/a_n=0.86$, is less than what would be expected based on calculated fits to data in heavier systems where, empirically, this ratio is found to be ≥1.[20] Using the same level-density parameters for fusion and fission results in calculated fission cross sections which are about twice that observed. Having different values for the two level-density parameters in heavier systems has been taken as evidence for shell effects,[20] and it is possible that a similar explanation could be developed for the lighter system studied here. Certainly strong evidence of shell effects are seen in the fission mass dependence.

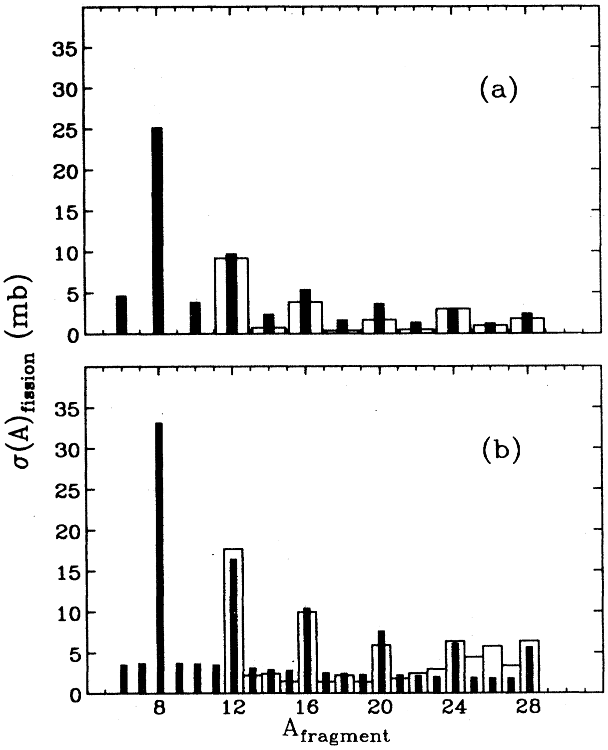

FIG. 12. Comparison of the predicted mass distributions using the statistical fission model discussed in the text (solid histograms) with the experimental results (open histograms) at $E_{\mathrm{c.m.}}=51.6$ and 60.5 MeV.

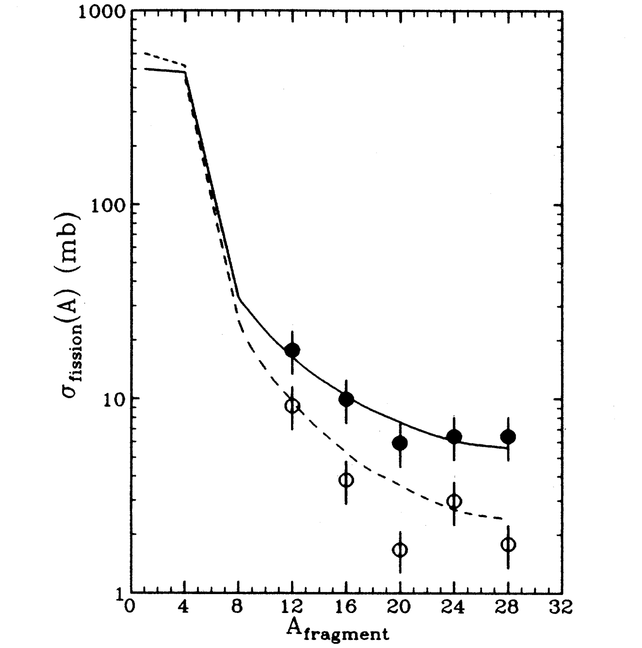

FIG. 13. Experimental cross sections for the stronger breakup channels at $E_{\text{c.m.}} = 51.6$ (open circles) and 60.5 MeV (solid circles). The results of the statistical fission model discussed in the text for these strong channels are also indicated by the dashed and solid curves, corresponding to the lower- and higher-energy data, respectively.

In principle, the Hauser-Feshbach and transition-state models might be expected to give similar predictions for heavy-fragment emission from the relatively light, ^{56}Ni system,[21,30] thus making the discontinuous behavior observed in the calculations shown in Fig. 13 surprising at first glance. It should be noted, however, that the simplifying assumptions commonly employed in actual calculations for the two models are quite different. Hauser-Feshbach calculations typically assume the emergence of two spherical fragments in the exit channel, with the transmission coefficients calculated for the ground states of these fragments using optical potentials. Our saddle-point calculations indicate that this assumption of spherical fragments is poorly met for the heavier mass fragments. Alternatively, the transition-state model as used here, although accounting for fragment deformation, employs a simplified, step function for the transmission coefficients—a poor assumption for the emission of light particles. The unified nature of fission and light-particle emission has been discussed by Moretto,[21] and there has been a recent effort to develop an "extended" Hauser-Feshbach model[37,38] which treats light-particle emission and heavy-fragment emission in a similar manner. This latter model differs from the transition-state calculations by using the scission point rather than the saddle-point phase space in determining the decay probabilities, but in light systems the difference between these should not be large. The apparent discontinuous behavior in the experimental mass distribution for $4 < A_{\text{fragment}} < 12$ (more data are needed for the $A = 8$ channel to confirm this)

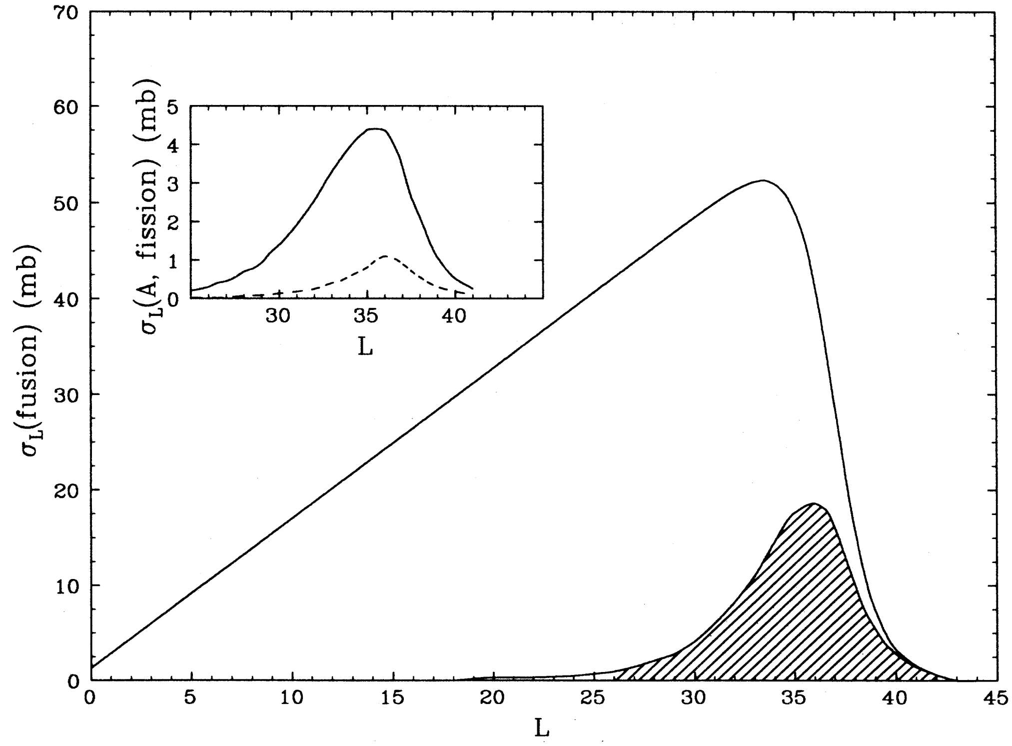

FIG. 14. Partial wave distribution for fusion (solid curve) and fission (shaded region) as indicated in the fission-model calculation. The inset shows the calculated partial wave distribution for the ^{8}Be (solid curve) and ^{28}Si channels (dashed curve).

may indicate a sudden onset of effects resulting from nuclear deformation for fragments with $A>4$; if so, this would again suggest the importance of shell effects on the detailed features of the mass dependence.

One feature of the transition-state calculations is that fission is restricted to the highest compound-nucleus spin values. Figure 14 shows the partial fusion cross-section distribution for the ^{32}S+^{24}Mg reaction at $E_{\mathrm{c.m.}}=60.5$ MeV, along with the component of the cross section which is predicted to lead to breakup fragments of mass $A\geq 6$. The basis for this behavior can be traced to the spin-dependent saddle-point energies (see Fig. 11). At lower spin values the saddle-point energies increase rapidly, going from the extreme asymmetry values (i.e., p, n, α decay) to the more symmetric mass channels, and thus heavy-fragment breakup is unlikely. At higher spin values the mass-asymmetry dependence of the fission barriers is substantially less, placing less of a penalty on heavy-fragment emission. This picture would suggest a spin dependence for the breakup to a given fission channel, with the more asymmetric fission channels starting at lower spin. Some indication for this is seen in the figure where the partial cross sections for fissioning to the mass 8 and symmetric mass 28 channels are shown, although the range of partial waves where fission occurs is still found to be quite limited.

VII. DEEP-INELASTIC SCATTERING MODELS

In Sec. VI it was shown that the observed fully damped, binary reactions can be understood in terms of the fission decay of the equilibrated ^{56}Ni compound nucleus. In this section we will discuss possible alternative models where these yields are described in terms of a deep-inelastic scattering process. First we present a semiclassical mass flow calculation which follows the energy dissipation encountered by the two colliding ions. From a previous calculation of this type, applied to the ^{16}O+^{40}Ca reaction,[7] we would not expect to find a good description of the fully damped processes, but can hope for some insight into the behavior of the near-projectile-target breakup channels at forward angles. As an alternative approach we will also discuss the equilibrium model for orbiting as developed by Shivakumar *et al.*[8,10] This picture has been successfully used in describing fully damped processes in lighter systems ($A\leq 42$).

A. Semiclassical mass flow calculation

To simulate the mass flow of the interacting ^{32}S and ^{24}Mg ions in a deep-inelastic scattering process we made use of the computer code developed by Feldmeier.[39] This semiclassical calculation follows the interacting nuclei as they come together, form a connecting neck, and then either reseparate or fuse into a compound nucleus. Before contact the dissipative force is given by Randrup's window formula.[40] After the neck forms, one-body dissipation is introduced by a combination of the wall and window formulations.[41] The calculation results in estimates of the mean and variance of the mass drift, the final total kinetic energy, and the scattering angle as functions of the impact parameter.

The total kinetic energy $E_{K,\mathrm{tot}}$ and scattering angle values calculated for different impact parameters of the ^{32}S+^{24}Mg reaction at $E_{\mathrm{c.m.}}=60.5$ MeV are shown in Fig. 15. From these calculations one finds that for partial waves l less than $38\hbar$ the interacting nuclei stick together and do not reseparate for at least three full rotations, at which point the calculation stops and assumes the system has fused. The deep-inelastic component is then localized to spins $38\leq l\leq 42\hbar$ and to center-of-mass angles between $0°\leq\theta_{\mathrm{c.m.}}\leq 28°$. The mass drift from the projectile-target mass asymmetry increases with decreasing l, but even for $l=38\hbar$ the dispersion remains quite small ($\sigma_A/A\sim 0.09$) and the final mass asymmetry is expected to be very close to that of the entrance channel. Qualitatively, the forward rise in the observed values of $d\sigma/d\theta$ and $\langle E_{K,\mathrm{tot}}\rangle$ seen in Figs. 4 and 5, respectively, for the symmetric $A=28$ channel is consistent with these predictions, although the angle at which an equilibrium condition is met (i.e., constant values of $d\sigma/d\theta$ and $\langle E_{K,\mathrm{tot}}\rangle$) is somewhat larger than predicted. It is clear, however, that these calculations are unable to describe the fully damped cross sections. This is discussed further in Ref. 7.

B. Equilibrium model for orbiting

An alternative approach to the deep-inelastic scattering problem has been developed by Shivakumar *et al.*[8,10] in discussing fully damped processes for light systems. This equilibrium model gives a unified description of the

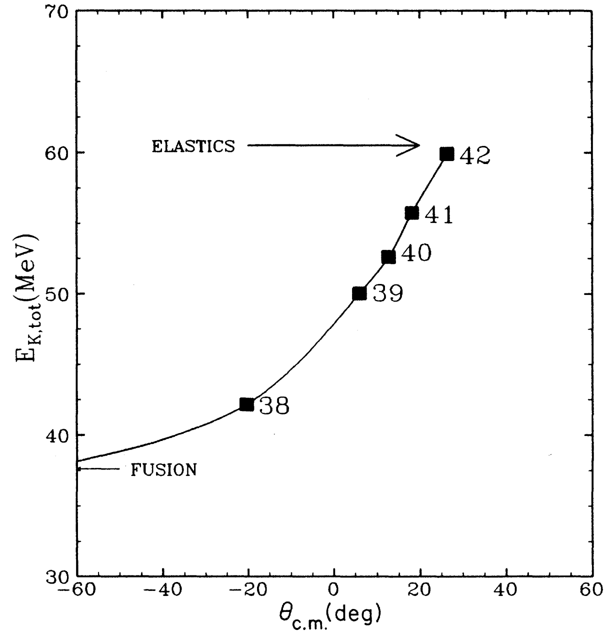

FIG. 15. Locus of final total kinetic energy and reaction angle as a function of the reaction partial wave for the ^{32}S+^{24}Mg reaction at $E_{\mathrm{c.m.}}=60.5$ MeV using the deep-inelastic scattering model discussed in the text. The position on the trajectory for l values between 38 and 42, inclusive, are indicated.

fusion and deep-inelastic orbiting processes, where the orbiting configuration, viewed in terms of the formation of a long-lived dinuclear complex, can act as a doorway to the formation of an equilibrated compound nucleus. The orbiting yield then corresponds to the fragmentation of the dinuclear complex during the early stages of the interaction, while longer-lived complexes relax towards fusion. In the equilibrium description of the orbiting process it is assumed that the final observables (mass distributions, angular distributions, $\langle E_{K,\mathrm{tot}} \rangle$) are determined after the dinuclear complex has held together long enough for the relevant degrees of freedom to reach equilibrium. The model differs from a fusion-fission picture in the assumption of an extended, equilibrated dinuclear complex being formed which never relaxes its shape to that of the compound nucleus. A detailed description of the orbiting model with examples of its application can be found in Refs. 8 and 10.

In applying this model to lighter systems it has been found that the adjustment of a single strength parameter in the Bass parametrization[42,43] of the nuclear potential energy leads to good agreement with the mass dependence of the dinuclear yields, the corresponding $\langle E_{K,\mathrm{tot}} \rangle$ values, and the total fusion cross section for these systems. The authors suggest that the Bass potential could be adjusted by either looking at the $\langle E_{K,\mathrm{tot}} \rangle$ values or the total fusion cross sections. In Fig. 16 the orbiting calculation results for the ^{32}S+^{24}Mg reaction at $E_{\mathrm{c.m.}}=60.5$ MeV are shown where the strength parameter A in the Bass parametrization has been adjusted: the solid histograms indicate the results of fitting the total fusion cross section with $A=0.037$ MeV^{-1}, and the crosshatched histograms are obtained by fitting the observed $\langle E_{K,\mathrm{tot}} \rangle$ values with $A=0.063$ MeV^{-1}. (The other Bass potential parameters are the same as suggested in Ref. 42, i.e., using the notation of this reference, $B=0.0061$ MeV^{-1}, $d_1=3.30$ fm, $d_2=0.65$ fm, $a=1.16$ fm, $b^2/a=1.39$ fm. Within this set of potential parameters, $A=0.048$ MeV^{-1}.) From inspection of this figure it is clear that this particular orbiting calculation does not reproduce the ^{32}S+^{24}Mg data. The experimental mass distribution is poorly reproduced in both calculations, and a consistent fit of the $\langle E_{K,\mathrm{tot}} \rangle$ values and the total fusion cross sections is not achieved.

It is possible that the poor agreement between theory and experiment in the ^{32}S+^{24}Mg case does not reflect a failure of the equilibrium orbiting model as much as the inadequacies of some of the simplifying assumptions (e.g., the use of ground-state Q values, taking spherical fragment shapes, and neglecting diffuse surface effects). The difficulty of obtaining a consistent fit to the total fusion cross section and the $\langle E_{K,\mathrm{tot}} \rangle$ values suggests that part of the problem may lie with the rotational energy term. Both diffuse-surface effects and fragment deformation will lead to greater moments of inertia and consequently will have the effect of lowering the rotation energy of the system. To test whether an improved fit could be achieved by introducing these effects, new calculations were performed where the diffuse-surface moments of inertia of two ellipsoidally deformed nascent fragments

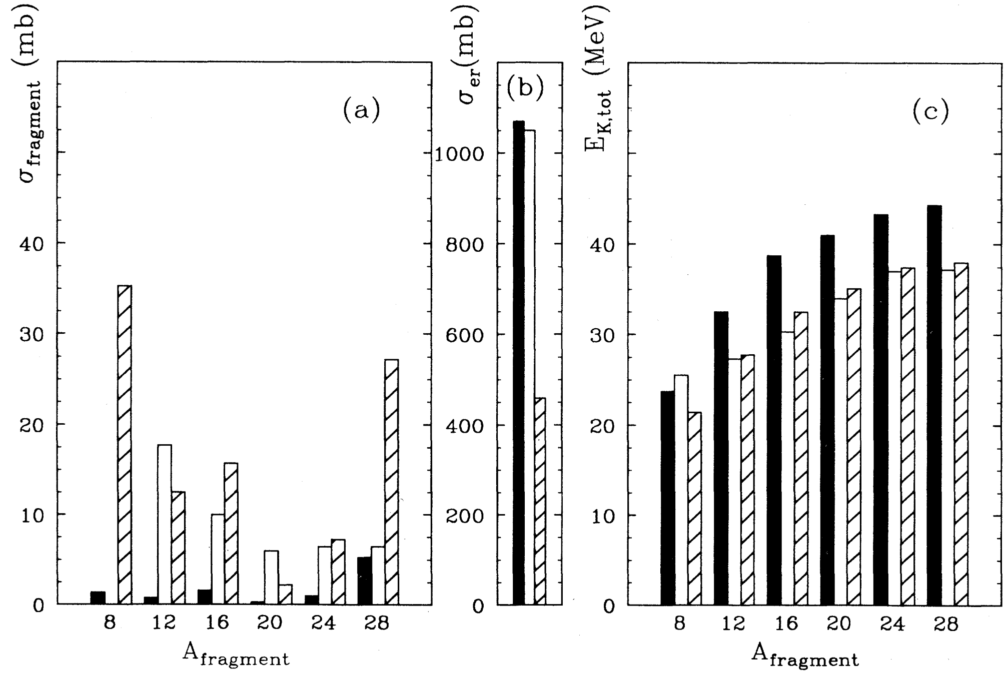

FIG. 16. Results of the equilibrium model for orbiting (solid and crosshatched histograms) compared to the data (open histograms) at $E_{\mathrm{c.m.}}=60.5$ MeV assuming two different values of the Bass potential strength parameter A (see text). The mass distributions (a), total fusion cross sections [(b) see Ref. 37], and total kinetic energies (c) are shown.

were used to calculate the generalized potential-energy surface.

The results of these calculations are compared to the data at the two beam energies in Figs. 17 and 18. We use the Bass parameters found above to fit the fusion cross section for the spherical fragment calculation with $A=0.037$ MeV^{-1}. The maximum angular momentum for fusion and orbiting processes is determined as before without allowing for deformation in the entrance channel (i.e., the calculations at $E_{\mathrm{c.m}}=60.5$ MeV use the same value of $l_{\mathrm{cr}}=36\hbar$ as found for the calculation shown by the solid histograms in Fig. 16). However, for the subsequent calculations of barrier energies an ellipsoidal deformation of $\beta=0.15$ is assumed for all fragments and the moments of inertia are corrected for the effect of having diffuse nuclear surfaces.[19] (This deformation is only slightly larger than suggested by symmetric saddle-point calculations where, to approximate the barrier for $l=36\hbar$, a deformation of $\beta=0.13$ is found.) The deformation dependence of the nuclear and Coulomb terms in the potential were taken as discussed in Ref. 43. These corrections lead to improved fits to the data with both the mass distributions and $\langle E_{K,\mathrm{tot}}\rangle$ values being reasonably well described. Part of the remaining discrepancy may be attributable to the use of ground-state Q values which strongly favor the ^{28}Si+^{28}Si channel ($Q_0=3.0$ MeV).

To achieve this agreement, however, it has been necessary to modify the generalized potential-energy surface by making the barriers more similar to the nuclear saddle-point barriers. The similarity of the results for the fusion-fission and orbiting calculations are perhaps, then, not too surprising and may be traced to the similarity between the saddle-point shapes of light systems and those of touching spheroids. For systems of total mass $A\leq 42$ additional evidence taken to support an orbiting interpretation include measurements of the entrance-channel dependence,[44] spin alignment,[17] lifetime effects,[45] and parity dependence[16] of the reaction yields. In general, however, these analyses assume a particular phase space for the fission process, corresponding to a post-scission configuration, in ruling out a possible fission contribution. Thus, it can be questioned whether the fission process is being properly accounted for in these systems. Some of these measurements have also been performed in systems which have been shown to manifest molecular-resonance behavior,[26] an additional complication which has been ignored in the analysis. Although an orbiting contribution is not needed to describe the present results, the possibility of such a contribution cannot be excluded.

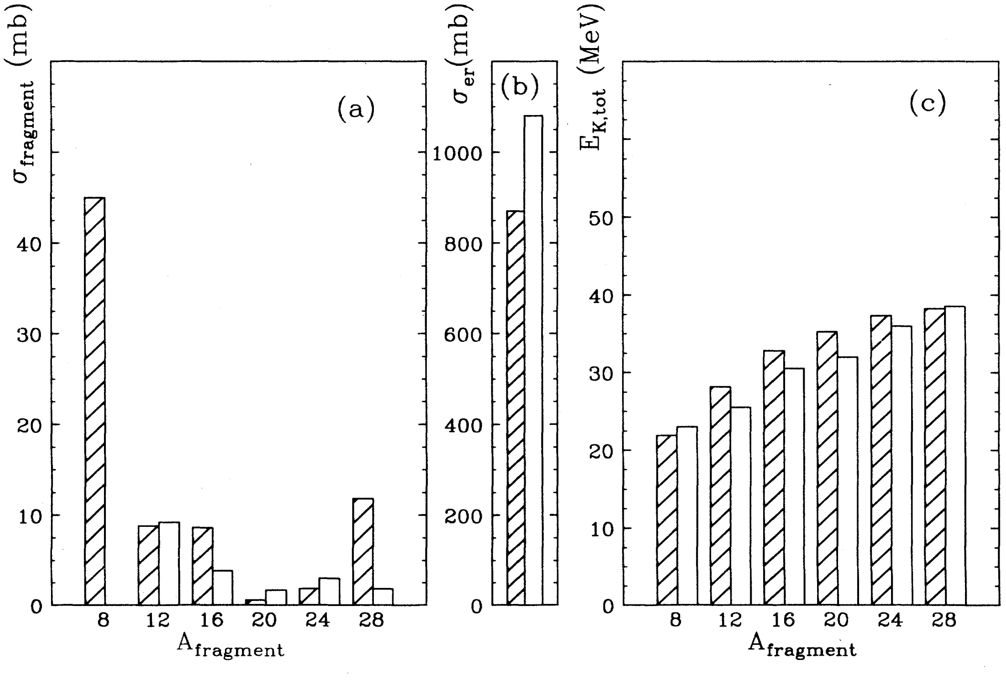

FIG. 17. Results of the equilibrium model for orbiting (crosshatched histograms) compared to the data (open histograms) at $E_{\mathrm{c.m.}}=51.6$. Nascent fragment deformations of $\beta=0.132$ are assumed (see text). The mass distributions (a) total fusion cross sections [(b); see Ref. 37], and total kinetic energies (c) are shown.

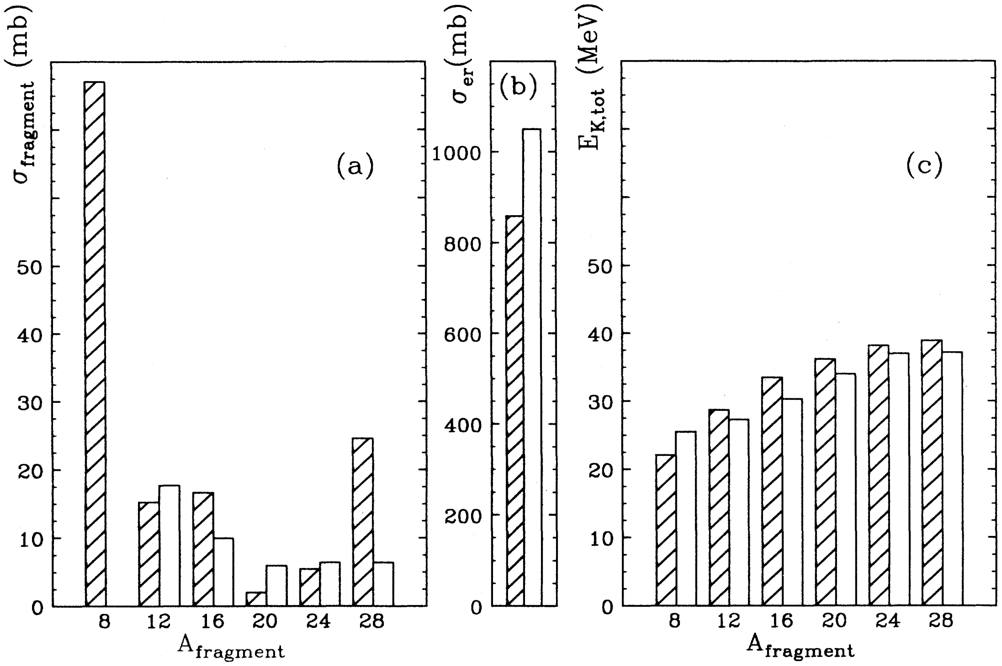

FIG. 18. Results of the equilibrium model for orbiting (crosshatched histograms) compared to the data (open histograms) at $E_{c.m.} = 60.5$. Nascent fragment deformations of $\beta = 0.15$ are assumed (see text). The mass distributions (a), total fusion cross sections [(b); see Ref. 37], and total kinetic energies (c) are shown.

VIII. SUMMARY AND CONCLUSIONS

The fully damped, binary reaction channels from the $^{32}S + ^{24}Mg$ reaction at $E_{c.m.} = 51.6$ and 60.5 MeV (corresponding to 1.8 and 2.2 times the Coulomb barrier, respectively) have been studied in a kinematically complete measurement. The angular dependence of the cross sections and average total kinetic energies $\langle E_{K,tot} \rangle$ in the two-body exit channels have been measured. The primary mass distribution, prior to secondary light-particle emission, of the breakup of the compound system has been derived. The data indicate that the mass-asymmetric breakup of the compound system is favored over symmetric fission.

The cross section for producing ^8Be fragments in the ground state at the two beam energies have been determined, and very rough limits found for the total ^8Be cross sections. The ^8Be channel is very interesting as it links the heavier fission fragment and light-particle evaporation channels; further measurement will be needed, however, to fully assess the importance of this channel.

A forward-angle rise in the cross sections and $\langle E_{K,tot} \rangle$ values seen in the mass $A = 24$ and 28 channels is found to be qualitatively consistent with the predictions of deep-inelastic, mass-flow calculations. These calculations are unable, however, to account for the fully damped processes.

In conclusion, significant cross sections, accounting for between 5 and 10% of the total fusion cross section, were found for the binary breakup of the compound system formed in the $^{32}S + ^{24}Mg$ reaction at energies of about twice the Coulomb barrier. These cross sections have been discussed in terms of (1) the transition-state model for fission and (2) the equilibrium model for orbiting. In the fission-model calculations of the ^{56}Ni breakup, the mass-asymmetric saddle-point energies, which include diffuse-surface and finite-nuclear-range effects, were used to determine the fission phase space. The success of the calculations in reproducing the main characteristics of the data suggest that the current macroscopic-energy calculations are applicable in light systems without major parameter adjustment. Equilibrium orbiting-model calculations with conventional parameters fail to reproduce the data. A shape for the orbiting, dinuclear complex corresponding to two aligned, deformed spheroids had to be assumed in order to obtain reasonable agreement with the data. This assumed shape is similar to that predicted for the saddle point in the fission calculation, suggesting a connection between the orbiting and fusion-fission calculations. While the presence of an orbiting process cannot be ruled out, the success of the conventional fusion-fission model strongly suggests that this process is responsible for the major fraction of the fully damped cross section in the $^{32}S + ^{24}Mg$ reaction. In any case, these damped, binary cross sections correspond to impact parameters which are intermediate between those responsible for the light-particle evaporation residues and those responsible for more peripheral, deep-inelastic processes. Studying the nuclear behavior for these partial waves is important for our understanding of the spin- and shape-dependent macroscopic-energy surfaces in light nuclei and the related limitations to fusion in these systems.

ACKNOWLEDGMENTS

The authors would like to thank F. W. Prosser for his comments on the manuscript. This work was supported in part by the U.S. Department of Energy, Nuclear Physics Divisions, under Contract No. W-31-109-ENG-38.

---

[*] Present address: Centre de Recherches Nucleaires, Strasbourg, France.

[†] Present address: Lawrence Livermore National Laboratory, Livermore, CA 94550.

[1] D. Shapira, J. L. C. Ford, Jr., J. Gomez del Campo, R. G. Stokstad, and R. M. DeVries, Phys. Rev. Lett. **43**, 1781 (1979).

[2] D. Shapira, R. Novotny, Y. D. Chan, K. A. Erb, J. L. C. Ford, Jr., J. C. Peng, and J. D. Moses, Phys. Lett. **114B**, 111 (1982).

[3] D. Shapira, D. Schull, J. L. C. Ford, Jr., B. Shivakumar, R. L. Parks, R. A. Cecil, and S. T. Thornton, Phys. Rev. Lett. **53**, 1634 (1984).

[4] K. Grotowski, Z. Majka, R. Płaneta, and M. Szczodrak, Y. Chan, G. Guarino, L. G. Moretto, D. J. Morrissey, L. G. Sobotka, R. G. Stokstad, I. Tserruya, S. Wald, and G. J. Wozniak, Phys. Rev. C **30**, 1214 (1984).

[5] R. Ritzka, W. Dünnweber, A. Glaesner, W. Hering, H. Puchta, and W. Trautmann, Phys. Rev. C **31**, 133 (1985).

[6] T. C. Awes, R. L. Ferguson, R. Novotny, F. E. Obenshain, F. Plasil, V. Rauch, G. R. Young, and H. Sann, Phys. Rev. Lett. **55**, 1062 (1985).

[7] S. J. Sanders, R. R. Betts, I. Ahmad, K. T. Lesko, S. Saini, B. D. Wilkins, F. Videbaek, and B. K. Dichter, Phys. Rev. C **34**, 1746 (1986).

[8] B. Shivakumar, D. Shapira, P. H. Stelson, M. Beckerman, B. A. Harmon, K. Teh, and D. A. Bromley, Phys. Rev. Lett. **57**, 1211 (1986).

[9] R. Płaneta, P. Belery, J. Brzychczyk, P. Cohilis, Y. El Masri, Ch. Grégoire, K. Grotowski, Z. Majka, S. Micek, M. Szczodrak, A. Wieloch, and J. Albiński, Phys. Rev. C **34**, 512 (1986).

[10] B. Shivakumar, S. Ayik, B. A. Harmon, and D. Shapira, Phys. Rev. C **35**, 1730 (1987).

[11] S. J. Sanders, D. G. Kovar, B. B. Back, C. Beck, B. K. Dichter, D. Henderson, R. V. F. Janssens, J. G. Keller, S. Kaufman, T.-F. Wang, B. Wilkins, and F. Videback, Phys. Rev. Lett. **59**, 2856 (1987).

[12] J. Brzychczyk, K. Grotowski, Z. Majka, S. Micek, R. Płaneta, D. Fabris, K. Hagel, J. B. Natowitz, G. Nebbia, P. Belery, P. Cohilis, Y. El Masri, and Gh. Gregoire, Phys. Lett. B **194**, 473 (1987).

[13] A. Ray, S. Gil, M. Khandaker, D. D. Leach, D. K. Lock, and R. Vandenbosch, Phys. Rev. C **31**, 1573 (1985).

[14] D. Shapira, Phys. Rev. Lett. **61**, 2153 (1988).

[15] S. J. Sanders, D. G. Kovar, B. B. Back, C. Beck, B. K. Dichter, D. Henderson, R. V. F. Janssens, J. G. Keller, S. Kaufman, T.-F. Wang, B. Wilkins, and F. Videbaek, Phys. Rev. Lett. **61**, 2154 (1988).

[16] W. Dünnweber, A. Glaesner, W. Hering, D. Konnerth, R. Ritzka, W. Trombik, J. Czakański, and W. Zipper, Phys. Rev. Lett. **61**, 927 (1988).

[17] R. R. Betts, in *Proceedings of the Fifth Adriatic International Conference on Nuclear Physics, Hvar, Yugoslavia, 1984,* edited by N. Cindro, W. Greiner, and R. Caplar (World-Scientific, Singapore, 1984), p. 33.

[18] J. Błocki, K. Grotowski, R. Płaneta, and W. J. Światecki, Nucl. Phys. **A445**, 367 (1985).

[19] A. J. Sierk, Phys. Rev. C **33**, 2039 (1986), and computer programs BARFIT and MOMFIT described therein.

[20] R. Vandenbosch and J. R. Huizenga, *Nuclear Fission* (Academic, New York, 1973).

[21] L. G. Moretto, Nucl. Phys. **A247**, 211 (1975).

[22] S. J. Sanders, in *Proceedings of the International Symposium on Developments of Nuclear Cluster Dynamics, Sapporo, 1988* (World-Scientific, Singapore, 1989).

[23] A. Breskin, G. Charpak, and S. Majewski, Nucl. Instrum. Methods Phys. Res. **220**, 349 (1983).

[24] S. B. Kaufman, E. P. Steinberg, B. D. Wilkins, J. Unik, and A. J. Gorski, Nucl. Instrum. Methods **115**, 47 (1974).

[25] Code PTOLEMY, M. H. Macfarlane and S. C. Pieper, Argonne National Laboratory Informal Report No. ANL-76-11 Rev. 1, 1978 (unpublished).

[26] P. Braun-Munzinger and J. Barrette, Phys. Rep. **87**, 209 (1982).

[27] H. Morgenstern, W. Bohne, W. Galster, K. Grabisch, and A. Kyanowski, Phys. Rev. Lett. **52**, 1104 (1984).

[28] J. Gomez del Campo, J. A. Biggerstaff, R. A. Dayras, D. Shapira, A. H. Snell, P. H. Stelson, and R. G. Stokstad, Phys. Rev. C **29**, 1722 (1984), and references therein.

[29] D. J. Morrissey, W. Benenson, E. Kashy, B. Sherrill, A. D. Panagioutou, R. A. Blue, R. M. Ronningen, J. van der Plict, and H. Utsunomiya, Phys. Lett. **148B**, 423 (1984).

[30] R. Stokstad, in *Treatise on Heavy-Ion Science,* edited by D. Allan Bromley (Plenum, New York, 1985), Vol. 3, p. 83.

[31] J. R. Nix, Nucl. Phys. **A130**, 241 (1969); K. T. R. Davis and J. R. Nix, Phys. Rev. C **14**, 1977 (1976); H. J. Krappe, J. R. Nix, and A. J. Sierk, *ibid.* **20**, 992 (1979); K. T. R. Davies and A. J. Sierk, *ibid.* **31**, 915 (1985).

[32] K. T. R. Davies, R. A. Managan, J. R. Nix, and A. J. Sierk, Phys. Rev. C **16**, 1890 (1977).

[33] F. Pühlhofer, Nucl. Phys. **A280**, 267 (1977).

[34] P. Möller and J. R. Nix, At. Data Nucl. Data Tables **26**, 165 (1981).

[35] A. Bohr and B. R. Mottelson, *Nuclear Structure* (Benjamin, New York, 1969), Vol. 1.

[36] The total cross sections for fragments of mass $A \geq 40$ were found to be 1080 ± 130 and 1050 ± 100 mb at $E_{\mathrm{c.m.}}=51.6$ and 60.5 MeV, respectively. These values are in good agreement with the earlier work reported by D. G. Kovar, in *Proceedings of the IPCR Symposium on Macroscopic Features of Heavy-Ion Collisions and Pre-equilibrium Process,* edited by H. Kamitsubo and M. Ishihara (Hakone, Japan, 1977), p. 18.

[37] S. M. Lee, W. Yokota, and T. Matsuse, in Proceedings of the Symposium on the Many Facets of Heavy-Ion Fusion Reactions, 1986, edited by W. Henning, D. Kovar, S. Landowne, and S. Pieper (Argonne National Laboratory Report ANL-PHY-86-1, 1986, p. 63).

[38] T. Matsuse and S. M. Lee, in *Proceedings of the International*

Symposium on Developments of Nuclear Cluster Dynamics, Sapporo, 1988 (World-Scientific, Singapore, 1989), p. 312.

[39] H. T. Feldmeier, Argonne National Laboratory Report No. ANL-PHY-85-2, 1985 (unpublished).

[40] F. Beck, J. Blocki, M. Dworzecka, and G. Wolschin, Phys. Lett. **76B**, 35 (1978).

[41] J. Blocki, Y. Boneh, J. R. Nix, J. Randrup, M. Robel, A. J. Sierk, and W. J. Swiatecki, Ann. Phys. (N.Y.) **113**, 330 (1978).

[42] R. Bass, Phys. Rev. Lett. **39**, 265 (1977).

[43] R. Bass, Nucl. Phys. **A231**, 45 (1974).

[44] A. Ray, D. D. Leach, R. Vandenbosch, K. T. Lesko, and D. Shapira, Phys. Rev. Lett. **57**, 815 (1986).

[45] A. Glaesner, W. Dünnweber, W. Hering, D. Konnerth, R. Ritzka, R. Singh, and W. Trombik, Phys. Lett. **169B**, 153 (1986).